# Pore-Scale Saturation, Temperature, Pressure and Velocity Characterization of SAGD Process

Sahand Etemad[1], Arash Behrang[1], Apostolos Kantzas[1,2]
1. University of Calgary, Calgary, AB, Canada
2. PERM Inc. TIPM Laboratory, Calgary, AB, Canada

*This paper was prepared for presentation at the International Symposium of the Society of Core Analysts held in Vienna, Austria, 27 August – 1 September 2017.*

## ABSTRACT

In this paper, pore-scale phenomena in SAGD such as steam propagation and fingering as well as entrapment of oil behind the swept zone are visualized and evaluated. Using saturation, temperature, velocity and pressure profiles at the steam chamber edge and throughout the media, the interconnectivity of each parameter is discussed.

For this goal, a 2-D glass micromodel was reconstructed, binarized and meshed in COMSOL. Then the digital 2-D micromodel was fed into OpenFOAM, which is the open source CFD package of choice in this work. The mass and momentum conservation equations are used to model the fluid dynamic. For tackling the phase change, i.e. steam condensation and evaporation on the interface, within the simulation, the Lee phase change model was added to the pre-defined Volume of Fluid (VOF) based solver, compressibleMultiphaseInterFoam. The Lee model assumes that mass is transferred at a constant pressure due to temperature difference. For each phase in the multi-region model, sets of mass conservation, Navier-Stokes momentum and energy equations under non-isothermal conditions are solved simultaneously.

The results show connection between temperature, pressure, velocity and flow (saturation) profile. Sharp temperature gradient between steam and oil phase was observed, pressure profile throughout the medium shows pressure buildup behind the steam-oil interface, downward flowing of condensate and heated oil as well as upward and sideways propagation of steam was observed through flow streams and velocity profile component. Heat propagation within the media and viscosity reduction was investigated. Oil entrapment behind the swept zone as well as steam chamber growth is demonstrated and finally effect of steam additives on sweep efficiency and recovery factor was reported.

## INTRODUCTION

The increasing universal demand for energy and the decreasing conventional oil resources are the motivation for the study of heavy oil recovery. Total discovered bitumen in place is 4512 billion barrels worldwide which goes up to 5505 billion barrels with an additional 993 billion prospective barrels of natural bitumen recourses (Meyer *et al*., 2007). This source of energy has high viscosity and density and because of that primary recovery methods are not sufficient for production. The enhanced oil recovery methods can be classified into thermal and/or solvent displacements, chemical, polymer flooding, micellar flooding and microbial methods (Hart, 2014). In thermal methods, oil viscosity will

decrease several orders of magnitude by increasing the formation temperature (Butler *et al*., 1981). Typical thermal recovery methods can be classified into steam flooding, cyclic steam stimulation (CSS) and steam-assisted gravity drainage (SAGD) (Butler, 1997; Butler *et al*., 1981). SAGD, has a high recovery factor and relatively low environmental footprint and is widely used. However, pore-scale phenomena have to be investigated deeply as they lead to a better understanding of macroscopic observations in the field, (Al-Bahlani and Babadagli, 2009)

In SAGD, Figure 1, steam is injected into upper horizontal well, propagates vertically at the beginning and then flows toward the perimeter of the created steam chamber. This process can be described in the following stages: Continuous steam injection into the chamber, chamber growth upward and sideways, condensation of the steam on the interface between oil and steam and downward flow of the heated oil and condensate to the production well.

There are many uncertainties such as steam condensation on the interface, oil recovery, pressure distribution, fluid flow on the chamber and transition zone between oil and steam phases. Better understanding of the temperature, pressure, velocity and flow profiles is necessary for SAGD improvement. The SAGD process has been visually investigated both experimentally and through numerical simulation. Because of experimental complexities such as setting the boundary and initial conditions and continuous measurements throughout the medium, there is more attention toward numerical simulations to model SAGD at the grain level (Al-Bahlani and Babadagli, 2009) Simulation of SAGD in OpenFoam (Andersen, 2011) adding the phase change model to it, enables us to keep track of the velocity, pressure and temperature profile continually throughout the medium, steam chamber geometry.

In this work, SAGD is evaluated in a micromodel through numerical simulation and by visualizing flow, temperature, pressure and velocity profile. For this propose, a 2D micromodel with 390×390 $\mu m$ dimensions and square shaped grains was reconstructed and fed into the OpenFoam. Full T, P, V and optical mapping of the SAGD recovery experiment is performed.

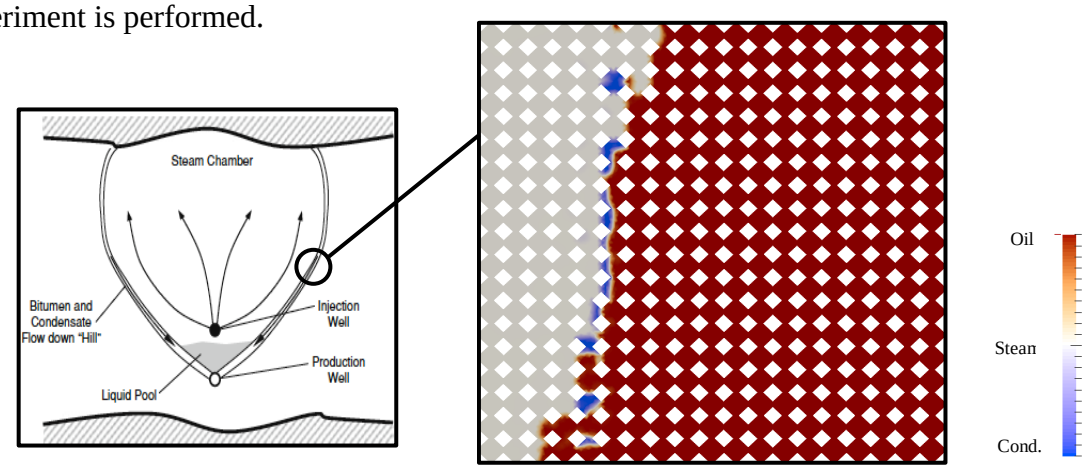


(a) (b)

Figure 1: SAGD, Field scale (Yang and Gates, 2009) (a), Pore Scale (b)

## METHODOLOGY

Lagrangian and Eulerian methods are two popular methods for fluid flow simulation. The limitation for Lagrangian methods is the restriction to simple cases (Lee *et al*., 2015). Therefore, for simulating complex geometries of the pore, methods based on Eulerian viewpoints will be used, Figure 2. For tackling two phase flow and capture the interface between phases, Volume of Fluid Method (VOF) and Level-Set (LS) methods are used. They are based on Eulerian point of view (Hirt and Nichols, 1981) (Osher and Sethian, 1988) (Peng *et al*., 1999). The LS method can capture complex interfaces but the drawback is the mass loss when solving the advection equation (Kartuzova and Kassemi, 2011) (Wang *et al*., 2008). In the VOF method, energy, momentum and mass equation is solved for each and every phase simultaneously (Hirt and Nichols, 1981). Sum of the volume fractions for all phases in a cell is equal to one, Figure 3. VOF is an interface tracking method and which is widely used in phase change problems. It is mass conservative (Hirt and Nichols, 1981) (Sussman and Puckett, 2000). As we can see from Figure 3, $\alpha$ (volume fraction), of each phase has a value between 0 and 1.

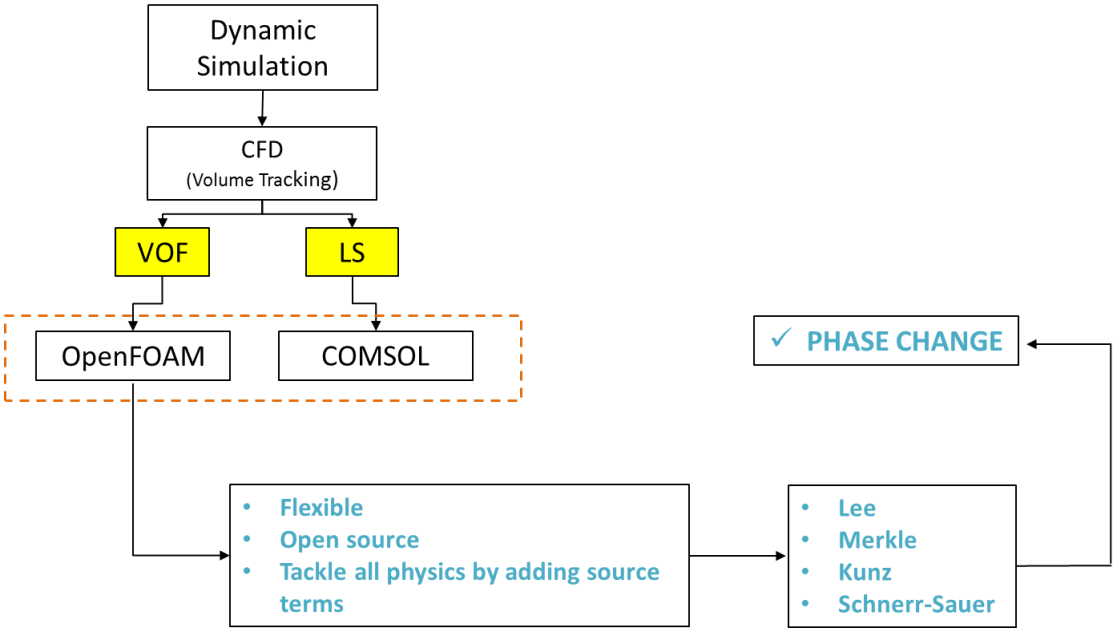


Figure 2: Pore level Modeling VOF method

"compressibleMultiphaseInterphasechangeFoam" is the solver we used for SAGD simulation in this work and is based on VOF method to compute the conservation equations for oil, condensate and vapor (Gueyffier *et al*., 1999). A single momentum equation is solved for three phases and the properties of the mixture are calculated based on the VOF method. Governing equations to model fluid flow and heat transfer in condensation/evaporation phenomena are mass, momentum and energy conservation. The governing equations are as follows:

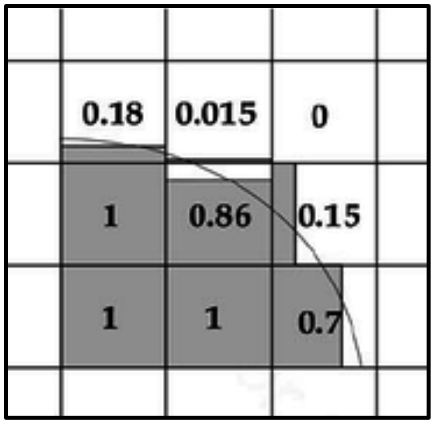


Figure 3: Schematic of alpha value in the cells close to the interface (VOF) (Martinez *et al*., 2006)

$$\sum_{i=oil,water,steam} \alpha_i = 1 \quad (1)$$

$$\alpha_{\text{oil}} = \frac{\text{oil volume}}{\text{total cell volume}} \quad \alpha_{\text{steam}} = \frac{\text{steam volume}}{\text{total cell volume}} \quad \alpha_{\text{water}} = \frac{\text{water volume}}{\text{total cell volume}} \quad (2)$$

The continuity equation for each phase (Kartuzova and Kassemi, 2011):

$$\frac{\partial(\alpha_i \rho_i)}{\partial t} + \underbrace{\nabla . \, [\alpha_i \rho_i \vec{u}]}_{flux\ of\ fluid} = S_{\alpha_i}, \quad i = oil, water, steam \quad (3)$$

Where $\rho$, $u$ and $t$ are density, velocity and time, respectively. $S_i$ is interfacial mass transfer:

$$S_{\alpha_l} = \dot{m}_i \, . \, A_i \quad (4)$$
$$S_{\alpha_v} = \dot{m}_i \, . \, A_i \quad (5)$$
And
$$A_i = |\nabla \alpha| \quad (6)$$

Where $A_i$ is the interfacial area density vector and $\dot{m}_i$ is mass flux vector which can be determined based on the proper phase change model, and $\alpha$ volume fraction of the primary phase (Schmidt and Grigull, 1989). In order to tackle phase change, we use LEE phase change model (Lee *et al*., 2015).

We use averaging for measuring properties of the mixture fluid in order to solve momentum and energy equation at the same time for mixture (Piro and Maki, 2013):

$$\rho = \sum_{i=oil,water,steam} \rho_i \alpha_i \quad (7)$$
$$\mu = \sum_{i=oil,water,steam} \mu_i \alpha_i \quad (8)$$

Momentum equation:

$$\overbrace{\underbrace{\frac{\partial(\rho\vec{u})}{\partial t}}_{Variation} + \underbrace{\nabla.(\rho\vec{u}\vec{u})}_{Convection}}^{Inertia\ per\ volume} = \overbrace{\underbrace{-\nabla \mathrm{P}}_{Internal\ force} + \underbrace{\nabla.[\mu(\nabla\vec{u} + \nabla\vec{u}^T)]}_{Diffusion}}^{Divergenve\ of\ stress} + \underbrace{\rho\vec{g}}_{External\ force} + \underbrace{\vec{F}}_{Volume\ force} \quad (9)$$

F is defined as follows:

$$F = \left[\sigma\kappa\boldsymbol{n} + \frac{d\sigma}{dT}\left(\sigma T - \boldsymbol{n}(\boldsymbol{n}.\nabla T)\right)\right]|\nabla\alpha|\frac{2\rho}{\rho_1+\rho_2} \quad (10)$$

Where $\kappa = -\nabla.\mathbf{n}$ and $\sigma$ are the curvature and surface tension terms, respectively.

Energy equation:

$$\frac{\partial(\rho C_p T)}{\partial t} + \nabla.\left(\underbrace{\vec{\boldsymbol{v}}(\rho E + P)}_{Flux\ of\ energy}\right) = \nabla.\left(\underbrace{k_{eff}\nabla T}_{\text{Energy transfer due to conduction}}\right) + \underbrace{Q}_{\text{volumetric heat sources}} \quad (11)$$

Where $Q$ is the volumetric heat sources, $k_{eff}$ is the thermal conductivity term given by:

$$k_{eff} = \sum_{i=oil,water,steam} k_{eff_i}\alpha_i \quad (12)$$

Using these equations, a new solver is developed in OpenFOAM solver in order to address the phase change problem.

The Lee phase change model (Lee *et al.*, 2015) was implemented into the solver "multiphasecmpressibleinterFoam" which is a VOF-based solver of the OpenFOAM package to take phase change into account in presence of steam, oil and condensate. This model assumes that phase change happens in constant pressure because of temperature gradient.

$$S_{\alpha_v} = -S_{\alpha_l} = r_l\alpha_l\rho_l\frac{T-T_{sat}}{T_{sat}} \quad T > T_{sat} \quad \text{evaporation process} \quad (13)$$

$$S_{\alpha_l} = -S_{\alpha_v} = r_v\alpha_v\rho_v\frac{T_{sat}-T}{T_{sat}} \quad T < T_{sat} \quad \text{condensation process} \quad (14)$$

where $S_{\alpha_v}$ and $S_{\alpha_l}$ are the interfacial mass transfer rates for vaporization and condensation respectively. $r$ denotes the mass transfer intensity factor with unit $s^{-1}$. The $r$ value is recommended to be as such to keep interfacial temperature close to saturation temperature, i.e. consistency between temperature and saturation profile. Researchers have used a very wide range of values for $r$, flow regime, geometry, mesh size and time steps. (Alizadehdakhel *et al.*, 2010; De Schepper *et al.*, 2009; Wu *et al.*, 2007) (Goodson *et al.*, 2010; Yang *et al.*, 2008). We sat $r_v = r_l$ = 1000 to get $T_i$ (interface temperature) close to $T_{sat}$.

## RESULTS

In this section, we will demonstrate saturation, temperature, velocity and pressure mapping throughout the geometry and in different time-steps. Analysis of the results and discussion of the correlation among all parameters, P, $\vec{V}$, T and $\alpha$ will follow.

Figure 4 shows snapshots for the simulation. Saturation, Temperature, Velocity and Pressure profiles in 9 different time steps (early stage to steam chamber development) are demonstrated in figure 4(a), 4(b), 4(c) and 4(d) respectively.

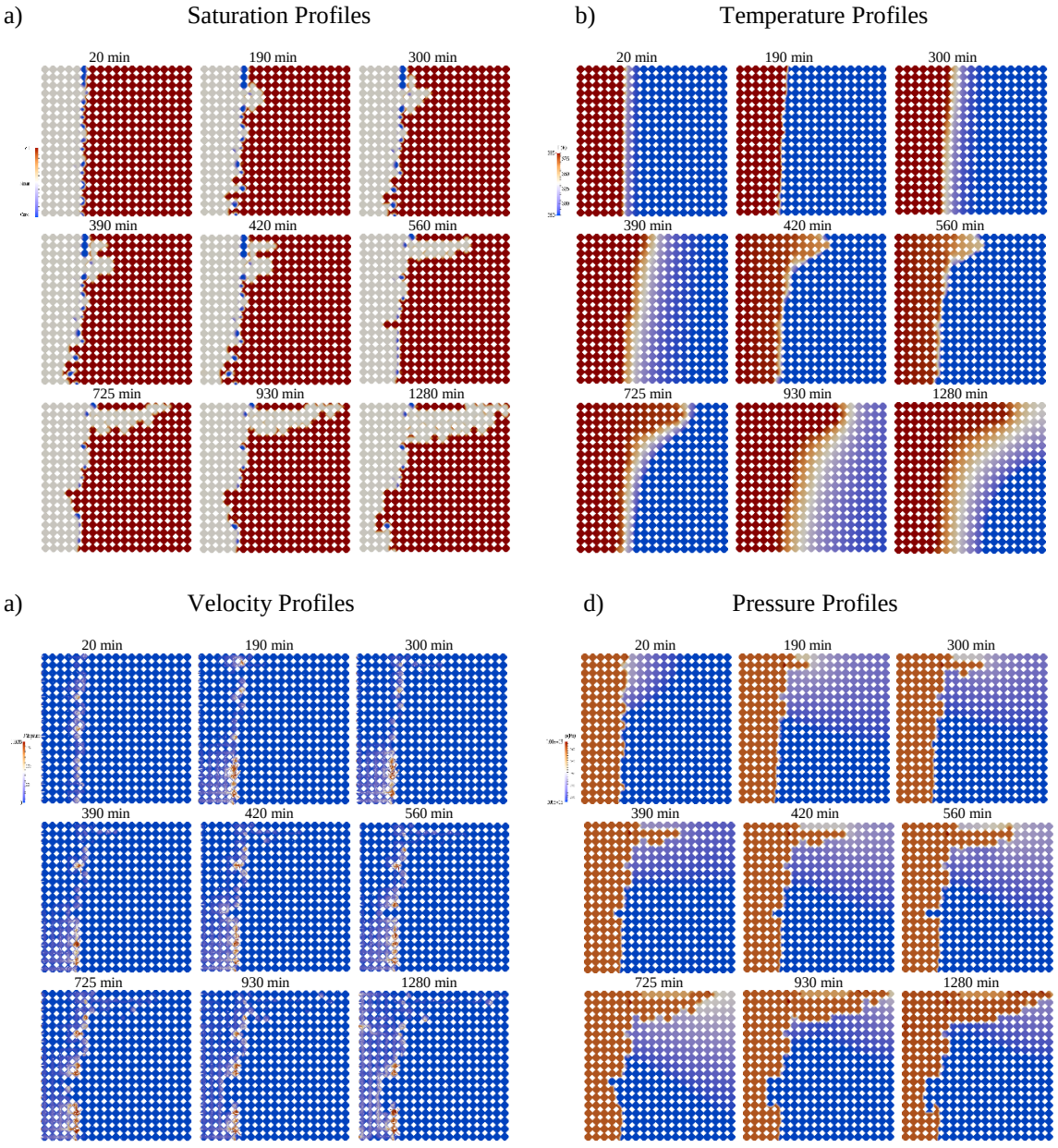


Figure 4: Saturation (a), Temperature (b), Velocity (c) and Pressure(d) profiles

The geometry was used in this work is a 2D reconstructed micromodel with square shaped grains which is based on the lab experiment, (Mohammadzadeh *et al*., 2010).

In this set of simulations, the system is initially saturated with steam at 385 K and oil in 280 K. The micromodel is supplied with steam from the left-hand side of the geometry and oil, condensate and steam production is from the bottom face. The system is at atmospheric pressure and $T_{sat} = 373\ K$.

Figure 4(a) is the saturation profile during the simulation in 9 different time-steps. As we can see, steam drains the oil out with a piston like trend at the beginning, from the beginning of the simulation until 190 min, later fingering of steam toward the right end of the geometry will be dominant, sideways propagation of the steam. Condensate with blue colour is generated on the interface between oil and steam. Oil is trapped locally in the swept zone. A blocking effect of the condensate on sweep efficiency of steam is observed. As we can see from the last three time-steps, steam is bypassing the lower part of the geometry because the condensate is blocking the steam from further propagation. We also observe local revaporization of the generated condensate. An example will be vaporizing the condensate phase partially from minute 420 to 560. In the real field, we have overburden heat loss because of the grains cooling down the steam, in these sets of simulations, the grains are not meshed and we do not have heat diffusion from the steam into the grains. Infinite amount of cold bitumen in the surrounding area in filed scale will results in more condensate generation while we have insulated boundaries for temperature here. We also have not included heat loss into the system. In the real experiment or field scale, the sealed faces are not fully insulated and lead to more condensation of steam.

Regarding steam chamber growth and steam phase fingering into the bitumen phase, upwards and sideways propagation of steam in real field data were observed (Ito and Ipek, 2005). In a sand pack experiments, steam fingering rather than a piston like propagation was observed as steam chamber grows (Butler and Dargie, 1994). Others (Sasaki *et al*., 2001) showed steam fingering in their 2D experimental model. The results of our simulation are consistent with these experiments as steam is propagating from the top of the micromodel and fingers towards the right end.

In terms of residual oil in the steam chamber behind the swept zone, Mohammadzadeh *et al.* (Mohammadzadeh *et al*., 2010) showed oil phase trapped behind the steam front in their 2D SAGD experiment on micromodel. Residual oil saturation inside the steam chamber is too low to be moved by steam phase, (Butler and Dargie, 1994). The results of our simulations show oil entrapment behind in the steam chamber which is immobile because of low saturation which agrees with the experimental data.

In Figure 4(b), the snapshots of temperature profile correspond to the previous 9 saturations have been demonstrated. High temperature steam with red color in the picture is cooling down on the interface, (white colour) and will be condensed. The reason will be the direct contact of steam with the oil phase which is in 280 K temperature. We see sharp temperature reduction on the interface. There is consistency between temperature and saturation profile as we compare the results from Figure 4(a) and 4(b). The interconnectivity will be having temperature close to the saturation temperature at the interface. As the simulation continues, high temperature is propagating from the top which is the steam fingering region. Condensate is generated on the interface which is the

transition zone where the temperature lays in between the steam and oil temperature, white colour on the temperature map.

Gates *et al.* showed temperature and saturation profiles of steam chamber from a simulation (Gates *et al*., 2005). Syed *et al.* mapped temperature profiles continuously through their micromodel using infrared camera in an experimental work (Syed *et al*., 2016). Mohammadzadeh *et al.* installed several thermocouples throughout their geometry and monitored temperature distribution (Mohammadzadeh *et al*., 2010). The conclusion was that the temperature profiles match the saturation profiles where temperature at the interface is close to saturation temperature. As we observe in the results section, temperature profile in our simulation is consistent with the saturation profile which agrees with the experimental observations above.

We also showed the results for velocity profile throughout the media in Figure 4(c). Initial steam injection velocity is $10^{-4}\frac{m}{s}$. Based on the velocity profile, the high velocity regions will be on the interface where droplets of condensate are generated and there is high convection velocity because of temperature difference, red colour on the velocity profile. Arrows show the directions of flow. Condensate and oil have downward flow and steam is propagating sideways, upward and downwards. The magnitude of the arrows represents the magnitude of the velocity. Due to higher viscosity for oil, the arrows are smaller in this region meaning the mobility toward production is lower in comparison to condensate and steam phases. As we go further from the steam, high temp region, the velocity vector will be smaller as the effect of temperature will be smaller. This will lead to smaller viscosity reduction and less mobility. When steam starts fingering from the top, the velocity vectors in this region will go higher in number and magnitude meaning that velocity toward the right end goes higher. Figure 5 shows a closer look of the velocity vectors in vicinity of the interface where the convection velocity between the phases with different temperatures is noticeable. In the steam phase on left side, there is propagation of steam in all directions and oil is getting mobilized only in vicinity of the steam phase and toward the production, bottom face. Figure 6 is a zoom-out view of the velocity vectors overlapping the saturation profile. Propagation of steam as well as convection velocity at the interface is noticeable.

Velocity profiles in our simulations show the flow of heated oil in the vicinity of the steam-oil interface. Away from the steam chamber, velocity vectors disappear, which means that oil will stay immobile. This is consistent with Butler's hypothesis that due to water condensation on the interface between steam and oil, major oil flow happens on the steam chamber because of interfacial tension support between oil and condensate as well as imbibition phenomena, (Butler and Dargie, 1994).

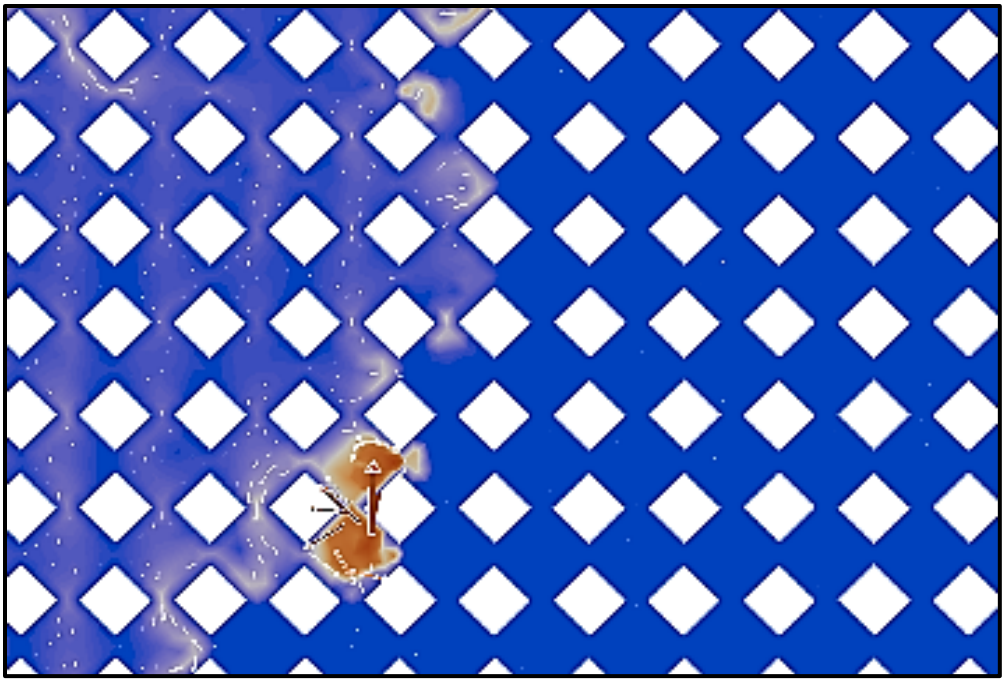

Figure 5: Zoom in view for the velocity vectors in vicinity of the interface

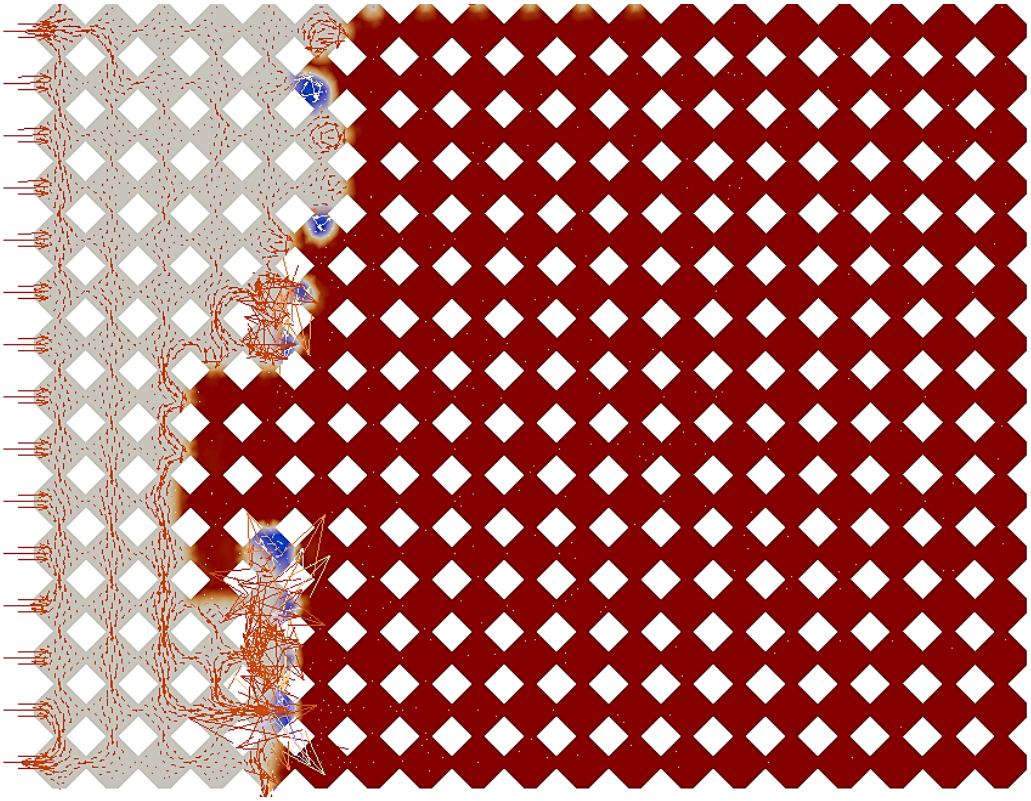

Figure 6: Zoom out view for the velocity vectors overlapping the saturation profile

Finally, Figure 4(d) shows the pressure profile during the simulation and is corresponds to the 9 time steps in saturation, temperature and velocity profiles. Pressure builds up behind the interface between oil and steam, 1.01 bar. The reason is the oil with higher viscosity which is blocking the steam from further proceeding until the pressure goes up and it has enough energy to pushes the oil toward the production site. System is initially sat to atmospheric pressure. During simulation, there is 200 Pa pressure difference between the oil and steam phases in maximum which is because of pressure buildup in the steam phase. Pressure profile is matched to the saturation and temperature profiles meaning that high pressure region is the steam region which is propagating from the top and has higher temperature respectively.

## CONCLUSION

SAGD simulation was conducted and saturation, temperature, pressure and velocity profiles were analyzed. It was concluded that steam is fingering from the top, condensate is generated on the interface, pressure builds up behind the swept zone and velocity is higher on the interface and lower in the oil region. Velocity, pressure, temperature and saturation profiles match with each other meaning that there is a sharp temperature, pressure and velocity gradient between oil and steam phases. Blocking effect of generated condensate as well as the re-vaporization of the condensate was observed. The velocity magnitude reported to be higher on the interface because of convection velocity due to high temperature gradient and condensation with higher density and lower viscosity in comparison to the oil.

Finally, it is critical to investigate effect of different parameters on SAGD performance and find and optimum state for the procedure. Effects of different mineralogy, injection rate, steam temperature and the understanding of SAGD thermodynamics to reduce heat losses in the process are priorities for future work. Running Solvent-SAGD simulation to reduce oil-water IFT for higher sweep efficiency as well as for improving heat efficiency will be another important task in the future.

## ACKNOWLEDGEMENTS

The authors gratefully acknowledge the financial support of the FUR program from NSERC, AITF/i-CORE, and the sponsoring companies: Athabasca Oil Corporation, Devon Canada, Foundation CMG, Husky Energy, Brion Energy, Canadian Natural, Laricina Energy, Maersk Oil, Suncor Energy, and Schulich School of Engineering (University of Calgary).

## REFERENCES

Al-Bahlani, A.-M., and T. Babadagli, 2009, SAGD laboratory experimental and numerical simulation studies: A review of current status and future issues: Journal of Petroleum Science and Engineering, v. 68, p. 135-150.

Alizadehdakhel, A., M. Rahimi, and A. A. Alsairafi, 2010, CFD modeling of flow and heat transfer in a thermosyphon: International Communications in Heat and Mass Transfer, **v. 37**, p. 312-318.

Andersen, M., Jarpner C, et al. 2011, A interphaseChangeFoam tutorial: Chalmers University of Technology, URL: http://www.openfoam.org/.

Butler, R., 1997, Thermal recovery of oil and bitumen, publ: GravDrain Inc.(2nd printing), Calgary, Alberta, 528pp.

Butler, R., G. McNab, and H. Lo, 1981, Theoretical studies on the gravity drainage of heavy oil during in‐situ steam heating: The Canadian journal of chemical engineering, **v. 59**, p. 455-460.

Butler, R. M., and B. Dargie, 1994, Horizontal wells for the recovery of oil, gas, and bitumen, Petroleum Socitey Monograph Number 2, Canadian Institute of Mining Metallurgy and Petroleum, University of Calgary.

De Schepper, S. C., G. J. Heynderickx, and G. B. Marin, 2009, Modeling the evaporation of a hydrocarbon feedstock in the convection section of a steam cracker: Computers & Chemical Engineering, **v. 33**, p. 122-132.

Gates, I. D., J. Kenny, I. L. Hernandez-Hdez, and G. L. Bunio, 2005, Steam injection strategy and energetics of steam-assisted gravity drainage: SPE International Thermal Operations and Heavy Oil Symposium.

Goodson, K., A. Rogacs, M. David, and C. Fang, 2010, Volume of fluid simulation of boiling two-phase flow in a vapor-venting microchannel: Frontiers in Heat and Mass Transfer (FHMT), **v. 1**.

Gueyffier, D., J. Li, A. Nadim, R. Scardovelli, and S. Zaleski, 1999, Volume-of-fluid interface tracking with smoothed surface stress methods for three-dimensional flows: Journal of Computational physics, **v. 152**, p. 423-456.

Hart, A., 2014, A review of technologies for transporting heavy crude oil and bitumen via pipelines: Journal of Petroleum Exploration and Production Technology, **v. 4**, p. 327-336.

Hirt, C. W., and B. D. Nichols, 1981, Volume of fluid (VOF) method for the dynamics of free boundaries: Journal of computational physics, **v. 39**, p. 201-225.

Ito, Y., and G. Ipek, 2005, Steam fingering phenomenon during SAGD process: SPE 97729 International Thermal Operations and Heavy Oil Symposium, Calgary, Nov. 1-3.

Kartuzova, O., and M. Kassemi, 2011, Modeling interfacial turbulent heat transfer during ventless pressurization of a large scale cryogenic storage tank in microgravity: 47th AIAA/ASME/SAE/ASEE Joint Propulsion Conference & Exhibit, p. 6037.

Lee, H., C. R. Kharangate, N. Mascarenhas, I. Park, and I. Mudawar, 2015, Experimental and computational investigation of vertical downflow condensation: International Journal of Heat and Mass Transfer, **v. 85**, p. 865-879.

Martinez, J., X. Chesneau, and B. Zeghmati, 2006, A new curvature technique calculation for surface tension contribution in PLIC-VOF method: Computational Mechanics, **v. 37**, p. 182-193.

Meyer, R. F., E. D. Attanasi, and P. A. Freeman, 2007, Heavy oil and natural bitumen resources in geological basins of the world: Open-File Report 2007–1084, US Geological Survey, Washington, DC. pubs.usgs.gov/of/2007/1084/ (accessed November 29, 2010).

Mohammadzadeh, O., N. Rezaei, and I. Chatzis, 2010, Pore-Level Investigation of Heavy Oil and Bitumen Recovery Using Solvent− Aided Steam Assisted Gravity Drainage (SA-SAGD) Process: Energy & Fuels, **v. 24**, p. 6327-6345.

Osher, S., and J. A. Sethian, 1988, Fronts propagating with curvature-dependent speed: algorithms based on Hamilton-Jacobi formulations: Journal of computational physics, **v. 79**, p. 12-49.

Peng, D., B. Merriman, S. Osher, H. Zhao, and M. Kang, 1999, A PDE-based fast local level set method: Journal of computational physics, **v. 155**, p. 410-438.

Piro, D. J., and K. J. Maki, 2013, An adaptive interface compression method for water entry and exit: Technical Report 2013-350, University of Michigan, Department of Naval Architecture and Marine Engineering. URL: http://deepblue.lib.umich.edu/handle/2027.42/97021.

Sasaki, K., S. Akibayashi, N. Yazawa, Q. Doan, and S. Ali, 2001, Experimental modelling of the steam-assisted gravity drainage process enhancing SAGD performance with periodic stimulation of the horizontal producer: SPE Jour, p. 189-197.

Schmidt, E., and U. Grigull, 1989, Properties of water and steam in SI-units: Springer, Berlin. Edition 4.

Sussman, M., and E. G. Puckett, 2000, A coupled level set and volume-of-fluid method for computing 3D and axisymmetric incompressible two-phase flows: Journal of Computational Physics, **v. 162**, p. 301-337.

Syed, A. H., N. Mosavat, J. Riordon, P. Lele, Z. Qi, M. Kim, H. Fadaei, A. Guerrero, and D. Sinton, 2016, A combined method for pore-scale optical and thermal characterization of SAGD: Journal of Petroleum Science and Engineering, **v. 146**, p. 866-873.

Wang, Z., J. Yang, and F. Stern, 2008, Comparison of particle level set and CLSVOF methods for interfacial flows: 46th AIAA Aerospace Sciences Meeting and Exhibit, Reno, Nevada.

Wu, H., X. Peng, P. Ye, and Y. E. Gong, 2007, Simulation of refrigerant flow boiling in serpentine tubes: International Journal of Heat and Mass Transfer, **v. 50**, p. 1186-1195.

Yang, X., and I. D. Gates, 2009, Design of hybrid steam-in situ combustion bitumen recovery processes: Natural resources research, **v. 18**, p. 213-233.

Yang, Z., X. Peng, and P. Ye, 2008, Numerical and experimental investigation of two phase flow during boiling in a coiled tube: International Journal of Heat and Mass Transfer, **v. 51**, p. 1003-1016.